Journal of Power Sources 480 (2020) 229122

Contents lists available at ScienceDirect

Journal of Power Sources

journal homepage: www.elsevier.com/locate/jpowsour

Investigating the degradation mechanism of the solid oxide fuel cell nickel-yttria stabilized zirconia anode under siloxane contamination

Jiashen Tian, Ryan J. Milcarek *

School for Engineering of Matter, Transport and Energy, Arizona State University, 501 E. Tyler Mall, Tempe, AZ, 85287, USA

HIGHLIGHTS

- SOFC degradation at 750 °C in different gas conditions with D4 siloxane is compared.
- Presence of water can reduce SOFC voltage degradation during siloxane contamination.
- Silicon deposition is associated with YSZ compared to Ni.
- Alternative mechanism for D4 contamination is proposed.
- Carbon deposition from D4 around Ni particles has role in degradation.

ARTICLE INFO

Keywords:
Solid oxide fuel cell (SOFC)
Siloxane
Biogas
Degradation
Contamination
Carbon deposition

ABSTRACT

In order to investigate the solid oxide fuel cell nickel-yttria stabilized zirconia (Ni-YSZ) anode degradation mechanism due to poisoning by Octamethylcyclotetrasiloxane (D4), four different experiments utilizing H_2+H_2O, H_2+H_2O+D4, H_2+D4 and H_2+CO+D4 as fuels at 750 °C are conducted in this study. The electrochemical characterization and morphology results are analyzed and compared for anode degradation phenomenon. The results contradict the previously proposed degradation mechanism as the experimental results show that water can inhibit the silicon deposition and anode degradation. Based on the experimental results in this study and previous studies about siloxane deposition on metal oxides, a new anode degradation mechanism is proposed. The proposed degradation mechanism for siloxane is due to siloxane adsorption resulting in silicon deposition and carbon deposition after siloxane decomposition.

1. Introduction

Water and Wastewater Treatment Plants (WWTPs) in the United States collectively demand around 2–4% of the total U.S. energy consumption representing a total cost of around $4.7 billion annually [1]. In 2011, 43% of U.S. WWTPs generated biogas using anaerobic digestion, but only 3.3% utilized the biogas to generate electricity via cogeneration or combined heat and power (CHP) [2]. Many WWTPs flare biogas, limiting energy recovery from this renewable resource. In this situation, utilizing a CHP system with solid oxide fuel cells (SOFCs) as power generator is a method to improve the energy efficiency of WWTPs. One pioneer application for an integrated biogas fuel cell system is the DEMOSOFC project in which a 175 kW SOFC plant with an electrical efficiency of 53% was installed in SMAT Collegno WWTP in the Turin area, Italy. The SOFC plant can supply around 30% of the WWTP electrical consumption and almost 100% of the thermal requirement [3]. Besides high energy conversion efficiency, the SOFC is also an environmentally friendly technology which can reduce the NO_x, SO_x and particulate matter emissions to the atmosphere [4]. However, the impurities in biogas will cause degradation of the SOFC [5].

The sources of biogas (landfills, WWTPs, farms), anaerobic digestion process, location, and season are all essential factors influencing the chemical composition of biogas. The main impurities of biogas include hydrogen sulfide (0.005–2 vol%), siloxanes (0–0.02 vol%), ammonia (<1 vol%), and halogenated compounds (<0.6 vol%) [6]. Most of these impurities, even at low concentrations, can potentially damage the prime mover of the CHP system [7,8]. Among these impurities, the prime movers are especially vulnerable to siloxane [9–11]. For SOFC, below 1 ppmv hydrogen sulfide concentration is generally considered a safe operating condition for SOFC [12]. However, H. Madi et al. [13]

* Corresponding author.
E-mail address: Ryan.Milcarek@asu.edu (R.J. Milcarek).

https://doi.org/10.1016/j.jpowsour.2020.229122
Received 24 August 2020; Received in revised form 9 October 2020; Accepted 25 October 2020
Available online 3 November 2020
0378-7753/

reported even ppb levels of siloxanes can cause fast degradation of SOFCs' Ni-YSZ (yttria-stabilized zirconia) anode. The average siloxane concentration in biogas of German WWTPs has been reported as 0.98 ppm [14] while the concentration can be as high as 41 ppm in WWTPs according to other sources [15].

The main siloxane species in biogas are classified as cyclic structure siloxanes, such as D4 (octamethylcyclotetrasiloxane) and D5 (decamethylcyclopentasiloxane), linear structure siloxanes, such as L3 (octamethyltrisiloxane) and L4 (decamethyltetrasiloxane), and other organosilicon compounds like TMS (Trimethylsilanol) [16]. Of the siloxane species, D5, D4 and D3 tend to have the highest concentrations among siloxanes in biogas from WWTPs [17]. Siloxane in WWTP biogas originates from silicones used in industrial processes, medical equipment, adhesives and consumer products [18]. During wastewater treatment siloxane is preferentially absorbed in the sludge flocs and volatize at temperatures above of 60 °C, which is common in the anaerobic digester [18]. Some of the siloxane compounds are more soluble in water and have higher vapor pressure (e.g., L2 and D3 siloxane) which makes them less likely to appear in biogas than others siloxanes (e.g., D4 and D5 siloxane) [12,18]. Anti-foaming agents, which are added to the anaerobic digester, are another common source of siloxane.

Ni-YSZ is one of the most extensively applied SOFC anodes due to excellent electrochemical and physical properties [19]. However, the mechanism of siloxane deposition in the Ni-YSZ SOFC anode has not been fully identified. K. Haga et al. [20] in 2008 assumed a two-step chemical reaction mechanism for D5 siloxane deposition. The two-step mechanism is shown in equations (1) and (2). In the first step, D5 undergoes a gas phase reforming reaction with water and converts the methyl groups to carbon monoxide and hydrogen. Then the remaining orthosilicic acid gas travels through the anode and decomposes to solid silicon dioxide and water.

$$[(CH_3)_2SiO]_5(g) + 25H_2O(g) \rightarrow 5Si(OH)_4(g) + 10CO(g) + 30H_2(g) \quad (1)$$

$$Si(OH)_4(g) \rightarrow SiO_2(s) + 2H_2O(g) \quad (2)$$

The mechanism proposed by K. Haga et al. was based on FESEM images and EDX results where silicon element was overlapped with oxygen element. In this case, the assumed Si deposition was reported as SiO_2, but not verified completely. Based on the assumed SiO_2 formation, anode poisoning by siloxane was classified as a deposition type mechanism [21] in which the Si accumulates in the anode. K. Haga et al. further claimed that silicon does not interact with Ni at 800 °C [22]. The researchers also proposed that the SiO_2 deposition in the anode would decrease the active triple phase boundary (TPB) area leading to higher anode polarization and ohmic loss [20]. However, Si deposition was found to be most significant near the anode surface with some occurring within the anode [20,21,23]. Thus, more research is needed to understand the mechanism of siloxane conversion and silicon deposition in SOFCs.

As shown by the summary of previous experiments in Table 1, the compositions of gases fed to the SOFC anode during siloxane contamination experiments tends to vary. For K. Haga and Kikuchi et al. experiments, besides H_2 and D5, only a small concentration of H_2O (3%) was added. However, in order to simulate syngas generated from biogas reforming, high concentrations of H_2O (~20%), CO (~10%) and CO_2 (~10%) were mixed with pure H_2 and D4 in the studies of H. Madi and D. Papurello et al. The experiments with syngas were meant to better simulate realistic operating conditions. According to equation (1) from K. Haga et al. components like H_2O would have an obvious influence on the degradation process. In this regard, a study focused on how individual components of syngas impact the siloxane deposition process in SOFC anode is necessary. It will also aid in understanding the siloxane poisoning mechanism of SOFC Ni-YSZ anode and provide a chance to verify the previously established theories. In order to compare with former studies, D4 was selected as siloxane contamination source.

Table 1
Summary of previous SOFC degradation studies due to siloxane.

Siloxane	Siloxane Conc. (ppm)	Temp. (°C)	Fuel	Anode	Ref
D5	10	800, 900, 1000	3% H_2O, 97%H_2	Ni-ScSZ	[20]
D5	60	800	3% H_2O, 97%H_2	Ni-ScSZ	[23]
D4	0.069, 0.1, 0.2, 0.25, 0.5, 1, 1.5, 2, 3	750	50% H_2, 20% H_2O, 20% CO, 10% CO_2	Ni-YSZ	[13]
D4	0.6, 3, 5	750	50% H_2, 20% H_2O, 20% CO, 10% CO_2	Ni-YSZ	[17]
D4	0, 0.111, 0.193, 0.47, 0.943, 1.447, 1923	750	50.8% H_2, 19.9% H_2O, 19.5% CO, 9.1% CO_2, 0.7% CH_4	Ni-YSZ	[5]

In this work, siloxane poisoning of Ni-YSZ anode is investigated in different gas compositions. The influence of H_2, H_2O, and CO on the D4 siloxane deposition process are assessed during long-term stability tests. Alternative mechanisms for siloxane deposition are proposed based on the experimental results.

2. Experimental setup

2.1. Fuel cell fabrication and characterization

The NiO + YSZ (60:40 w/w, Fuelcellmaterials) anode was prepared by dry pressing to prepare anode supported SOFCs (AS-SOFCs). The green body was then pre-sintering at 1100 °C for 4 h. After pre-sintering, yttria-stabilized zirconia (YSZ, $(ZrO_2)_{0.92}(Y_2O_3)_{0.08}$, Fuelcellmaterials) electrolyte was prepared by wet powder spray and also pre-sintering after spray. Then samarium doped ceria (SDC, $Sm_{0.20}Ce_{0.80}O_{2-X}$, Fuelcellmaterials) buffer layer was deposited by wet powder spray. After wet powder spray, anode, electrolyte and buffer layer were co-sintered at 1400 °C in air for 4 h. A lanthanum strontium cobalt ferrite (LSCF, $(La_{0.60}Sr_{0.40})_{0.95}Co_{0.20}Fe_{0.80}O_{3-x}$, Fuelcellmaterials) + SDC (7:3 w/w) cathode was spray deposited onto the SDC buffer layer by wet powder spray and then sintered to 1100 °C for 2 h [24,25]. The final anode thickness is ~380 μm, electrolyte thickness ~10 μm, buffer layer ~3 μm and cathode thickness ~17 μm. Silver paste was used for cathode current collector and the active area was 0.712 cm^2.

The fuel cell performance was measured by the I–V (current-voltage) method with 4-probe technique. The fuel cells open circuit voltage (OCV), polarization, power density, and operating voltage change at constant current density (V-t curve) were measured and recorded by the digital SourceMeter (Keithley 2460) interfaced with a computer.

An Electrochemical Impedance Analyzer (Solartron Analytical Energylab XM) was utilized to test the electrochemical impedance spectroscopy (EIS) of the fuel cells under OCV conditions. EIS was tested and recorded over a frequency range of 10^6 to 0.1 Hz with a signal amplitude of 10 mV.

2.2. Testing setup

Supplemental Fig. 1 shows the experiment setup. This experimental setup was built for investigating the Ni-YSZ anode SOFCs degradation due to D4 contamination in different atmospheres. A certified cylinder which includes pure N_2 carrier gas with precise concentration of D4 (5.743 ppm_v) was purchased and utilized. In order to adjust the D4 concentration in the fuels, but not change the other gas concentrations, the N_2+D4 gas was mixed with research grade N_2 gas to keep the total flow rate of N_2+D4 constant. In the experiment setup, the Brooks Delta II smart mass flow controllers (MFCs) interfaced with LabView software were utilized to mix the H_2, CO, N_2 and N_2+D4 with certain ratio at

atmospheric pressure. The NE-300 Just Infusion syringe pump (Pump-Systems Inc.) was utilized for supplying water into fuel deliver pipe. A heater was wrapped around the rest of gas deliver pipe for water vaporization. To confirm all the water was converted to steam and kept in gas phase, T-type thermocouples (Omega) were used to monitor the temperature of deliver pipe, which should be kept above 120 °C. To reduce the possibility of reactions between D4, water and the other gas components, D4 was incorporated into the mixture after the water heater and close to the furnace entrance.

Table 2 shows the gas flow rates, whose unit is standard cubic centimeters per minute (sccm), fed to anode side in different experiments. The total gas flow rate in anode side was fixed at 20 sccm to keep the same Reynolds number of flows. For all the experiments, to ensure the same number of electrons available for electrochemical conversion from the fuels, the H_2+CO total flow rate was kept at 7 sccm. Except the flow of N_2, the flow rates of H_2, CO, H_2O in all experiments were following the same component ratio in bio-syngas after reformer [13], respectively. For the cathode side, the air was supplied by natural convection through the vertical furnace.

For each experiment, a different Ni-YSZ anode SOFC was sealed on a quartz tube with silver paste. The setup was placed in a vertical tubular furnace, which was heated to 750 °C at 5 °C per minute. The experimental temperature was fixed at 750 °C for all the tests. The silver and steel wire were used for current collection and voltage measurement for the anode and cathode sides. A K-type thermocouple placed outside the SOFC was used for measuring the operating temperature. The anode of SOFCs were reduced roughly 3 h by 10 sccm H_2 and 10 sccm N_2.

2.3. Morphology analysis

After experiments, the fuel cell samples were crosscut to expose the cross-sections. Then the samples were embedded in epoxy to fill the pores in the anode. Cross-section sides were polished. SiC papers (from 46 μm to 16 μm) were used for coarse polishing. Fine polishing was achieved by water-based diamond suspension and colloidal silica diamond suspension (from 15 μm to 0.0415 μm). The cross section and micrographs of fuel cells' anode was conducted by a field emission scanning electron microscope (FESEM, JEOL JXA-8530F electron microprobe) with wavelength-dispersive spectrometers (WDS) which permits the measurement of elements from B through U, and provides qualitative silicon-trace analysis. In addition, this instrument is also equipped with an energy-dispersive spectrometer (EDS), which is capable of X-ray count rates in excess of 200 k counts per second and has high-speed X-ray mapping and quantitative microanalytical capabilities that rival the WDS. The SEM, EDS and WDX analysis were performed at 15 kV at 5×10^{-8} A beam current for the fuel cells' cross-section graphs and 15 kV at 2×10^{-8} A beam current for micrographs of anodes.

3. Results and discussions

3.1. Characterization of the SOFC

H. Madi et al. [13,14,17] reported that initial fuel cell degradation occurs prior to exposure to siloxane contamination and named this phenomenon as intrinsic degradation because of sources such as nickel grain growth and impurities in raw materials. The intrinsic degradation was also observed in this study. In order to reduce the impact of intrinsic degradation, the SOFCs were operating at their corresponding operating current densities for 50 h with clean fuel (i.e., no siloxane) to stabilize the performance before starting formal experiments. In order to concentrate on the degradation caused by D4, the voltage during reduction and intrinsic degradation during the first 50 h of operation was not shown. Then, except for the H_2+H_2O experiment, D4 with three different concentrations were mixed into the fuel with the sequence 1ppm$_v$, 0.4 ppm$_v$ and 2.5 ppm$_v$. To investigate how the concentration of siloxane impacts the degradation process, the sequence is neither increment nor decrement. The increment or decrement sequence which has been used in studies of H. Madi et al. [13,14,17] may not eliminate the time depended degradation influence on the experiment. Before and after each concentration, the polarization (I–V curve) and EIS tests were conducted. The SOFCs' operating voltage changes (V-t curve) at constant current density were recorded during the entire experiment. In previous SOFC siloxane degradation studies completed by H. Madi, D. Papurello, K. Haga et al. [5,13,20], the voltages selected for constant current density tests were relatively close to OCV (around 0.8–1 V), but not SOFCs' more common operating conditions (0.5–0.7 V). In this study, the current density was selected for the voltage range 0.5–0.7 V. In order to keep all SOFCs in similar electrochemical reaction equilibrium and voltage changes in real operating region, the initial operating voltages were fixed at ~0.65 V. The cell was then operated with clean fuel for 50 h, as discussed previously. Based on the fixed initial operating voltage, current densities for all experiments were around 300–350 mA cm^{-2}. The characterization tests results show in Supplemental Fig. 2, Fig. 1, Fig. 2, and Fig. 3, correspond to H_2+H_2O, H_2+H_2O+D4, H_2+D4, H_2+CO+D4 experiments, respectively. Supplemental Fig. 2, which assesses degradation with only H_2+H_2O, provides a baseline for comparison because no D4 is present.

In each figure, the SOFCs' performance degradation under D4 contamination can be noticed clearly from power density decrease and resistance increase. From the Nyquist plots part (c) and Bode plots part (d) in Supplemental Fig. 2, Figs. 1, Fig. 2, and Fig. 3, a small increase in mass transfer can be noticed at the low frequency arc ~1 Hz. Meanwhile, a small increase in ohmic resistance can be detected at high frequency. The main impedance increase occurred around 100 Hz attributing to anode activation degradation. An obvious impedance increase at cathode contribution frequency ~40 kHz [26] was not observed. In this case, no obvious LSCF cathode degradation influences this study. Generally, H_2+H_2O experiment has the lowest degradation and H_2+CO+D4 experiment has the highest degradation. To reveal the mechanisms of siloxane deposition, quantitative analysis is necessary. In order to compare the degradation between different experiments and between different concentrations in the same experiment, degradation rates were calculated and presented in Table 3, Table 4 and Table 5. The voltage degradation rates and resistance increase rates were used to evaluate the extent of degradation. In Table 3, the voltage degradation rates from V-t curves, which are directly correlated to the power densities' decrease, were used to represent the degradation rates of the SOFCs' performances.

In Table 4, area specific resistance (ASR) is reported from EIS results. The rate of resistance increase was calculated by equation (3) as follows:

$$(\text{Final Resistance Value} - \text{Initial Resistance Value}) / \text{Experiment Time} \quad (3)$$

After comparing all SOFCs' degradation results for different concentrations, a significant relationship between the D4 concentration and the degradation rate including voltage decrease and resistance increase have not been observed. To exclude the possibility that degradation originated from other sources beside D4, the H_2+H_2O, H_2+H_2O+D4 experimental results can be compared as evidence. Considering the

Table 2
Flow rate of anode side gases in different experiments.

Flow rates (sccm)	H_2	CO	H_2O	N_2 (D4 conc. 0/1/0.4/2.5 ppm)	D4+N_2 (D4 conc. 0/1/0.4/2.5 ppm)
H_2+H_2O	7	NA	2	11/11/11/11	NA/NA/NA/NA
H_2+D4	7	NA	NA	13/9.517/11.607/4.294	NA/3.483/1.393/8.706
H_2+CO + D4	5	2	NA	13/9.517/11.607/4.294	NA/3.483/1.393/8.706
H_2+H_2O + D4	7	NA	2	11/7.517/9.607/2.294	NA/3.483/1.393/8.706

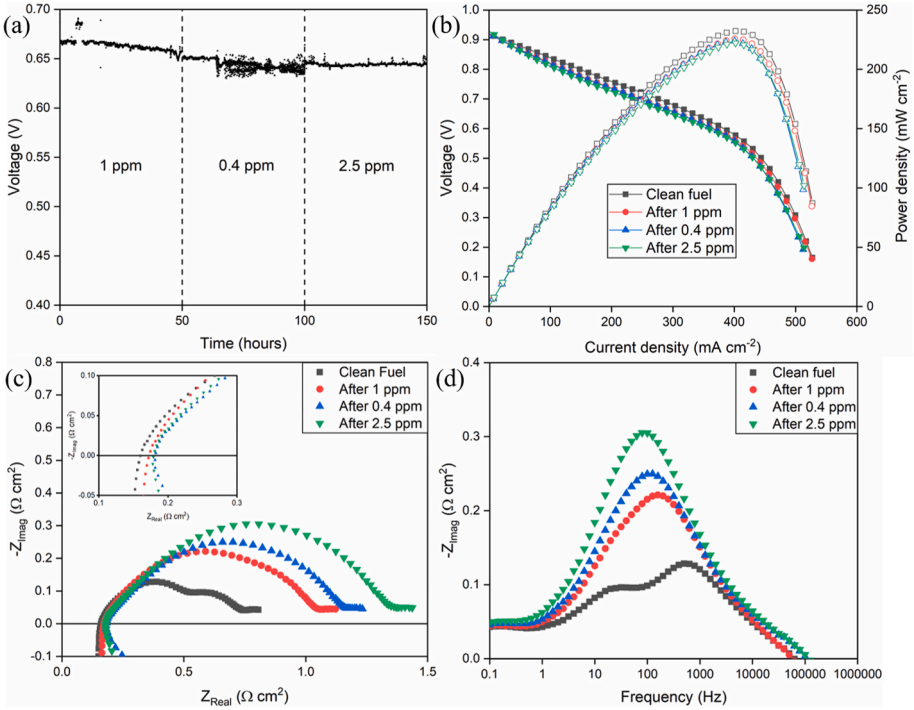

Fig. 1. Performance degradation of the SOFC under H_2+H_2O + D4 experiment. (a) The SOFC voltage at constant current density (300 mA cm^{-2}); (b) polarization curve; (c) Nyquist plots of EIS measurements; (d) Bode plots of EIS measurements. The clean fuel composition is H_2+H_2O + N_2 with no D4.

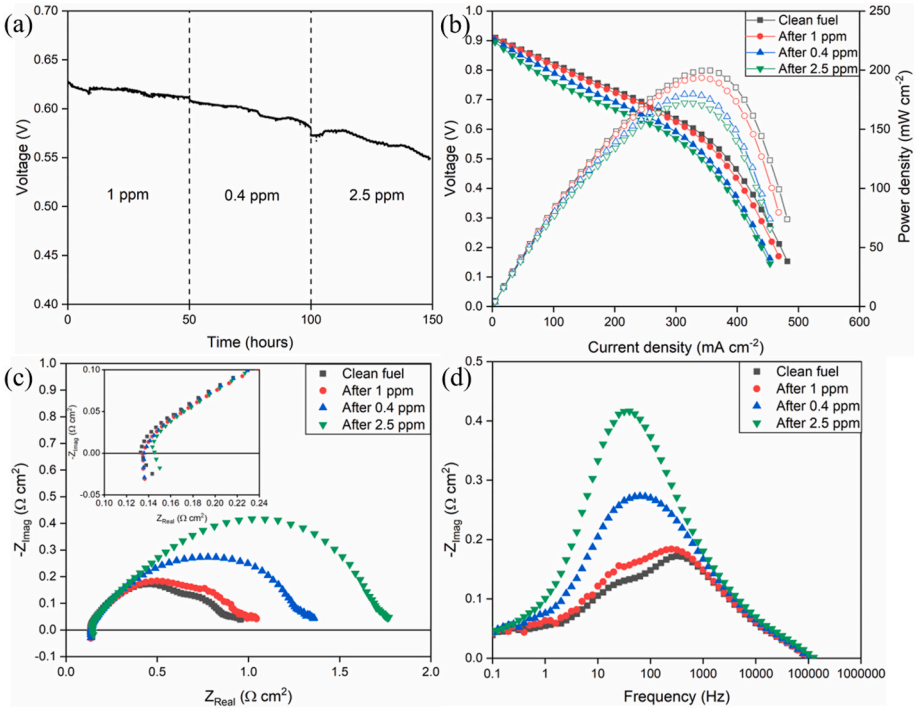

Fig. 2. Performance degradation of the SOFC under H_2+D4 experiment. (a) The SOFC voltage at constant current density (300 mA cm^{-2}); (b) polarization curve; (c) Nyquist plots of EIS measurements; (d) Bode plots of EIS measurements. The clean fuel composition is H_2+N_2 with no D4.

voltage degradation rates, at 1 ppm and 0.4 ppm D4 concentration, the H_2+H_2O+D_4 has a higher degradation rate. Furthermore, the total voltage degradation rate of the H_2+H_2O experiment is also smaller. The EIS results are another essential factor to compare. The results from Table 4 show that for the H_2+H_2O+D4 experiment, the rate of ASR increase is larger than the H_2+H_2O experiment. This indicates that D4 is the reason for the degradation. The reason why the concentration of siloxane did not result in a clearly observed change in degradation rate, which didn't appear in experimental results of H. Madi et al. [13], can be explained in different ways. Some of the degradation may be due to the LSCF cathode and SDC buffer layer used in this study which have non-negligible degradations during long-term operation [27], but that

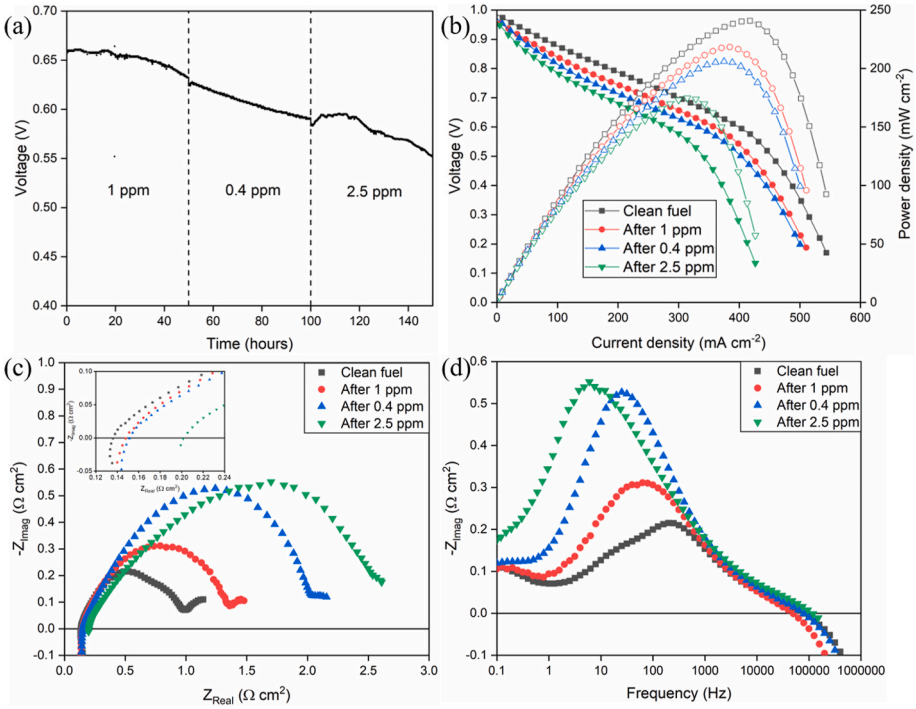

Fig. 3. Performance degradation of the SOFC under H_2+CO + D4 experiment. (a) The SOFC voltage at constant current density (350 mA cm^{-2}); (b) polarization curve; (c) Nyquist plots of EIS measurements; (d) Bode plots of EIS measurements. The clean fuel composition is H_2+CO + N_2 with no D4.

Table 3
Degradation rates calculated from V-t curve in different experiments.

Experiment	50 h (mV h^{-1})	100 h (mV h^{-1})	150 h (mV h^{-1})	Average (mV.h^{-1})
H_2+H_2O	0.08	0.1	0.08	0.08
Experiment	1 ppm D4/ 50 h (mV h^{-1})	0.4 ppm D4/ 100 h (mV h^{-1})	2.5 ppm D4/ 150 h (mV h^{-1})	Average (mV.h^{-1})
H_2+H_2O + D4	0.3	0.3	–	0.2
H_2+ D4	0.2	0.5	0.5	0.4
H_2+CO + D4	0.5	0.8	0.8	0.7

– No obvious voltage decrease.

Table 4
Area specific resistance (ASR) increasing rates calculated from EIS results in different experiments.

Experiment	50 h (mΩ cm^2 h^{-1})	100 h (mΩ cm^2 h^{-1})	150 h (mΩ cm^2 h^{-1})	Average (mΩ cm^2 h^{-1})
H_2+H_2O	0.1	1.1	9.5	3.6
Experiment	1 ppm D4/ 50 h (mΩ cm^2 h^{-1})	0.4 ppm D4/ 100 h (mΩ cm^2 h^{-1})	2.5 ppm D4/ 150 h (mΩ cm^2 h^{-1})	Average (mΩ cm^2 h^{-1})
H_2+H_2O + D4	6.4	2.2	3.6	4.1
H_2+D4	1.8	6.3	8.1	5.4
H_2+CO + D4	7.4	13.7	11.3	10.8

was not observed as a significant factor in the EIS results. As the cathode type and experimental conditions were the same in all experiments including the H_2+H_2O baseline experiment, the influence of cathode or buffer layer degradation can be excluded as a major contributing factor for the increased degradation with D4 exposure. The relatively short

Table 5
Ohmic resistance increasing rates calculated from EIS results in different experiments.

Experiment	50 h (mΩ cm^2 h^{-1})	100 h (mΩ cm^2 h^{-1})	150 h (mΩ cm^2 h^{-1})
H_2+H_2O	0.2	–	0.03
Experiment	1 ppm D4/50 h (mΩ cm^2 h^{-1})	0.4 ppm D4/100 h (mΩ cm^2 h^{-1})	2.5 ppm D4/150 h (mΩ cm^2 h^{-1})
H_2+H_2O + D4	0.2	0.2	–
H_2+D4	0.04	0.02	0.3
H_2+CO + D4	0.2	0.07	1.1

– No obvious ohmic resistance increase.

time operating with only hydrogen prior to D4 testing (~50 h) may be insufficient. The size of SOFCs whose active area is 0.712 cm^2 in this study is much smaller than previous studies from H. Madi et al. [13] with 12.5 cm^2 active areas. The SOFCs' size difference may influence the siloxane deposition speed as well. Although the connection between D4 concentrations and degradation was not observed, the degradation due to siloxane poisoning in different experiments shows time dependent behavior, generally.

According to Tables 3 and 4, the H_2+D_4 and H_2+D4+CO experiments shared the similar degradation trend that degradation rates were relatively small at the beginning and increased with time. One interesting result can be pointed out is that changes in the ohmic resistance followed the D4 concentration trends. This can be proved by calculation results shown Table 5. For H_2+H_2O+D_4 experiment and the baseline H_2+H_2O experiment, there was relatively large degradation rate initially which decreased with time. The high concentration of water in the fuel may react with D4 in the anode and this may be responsible for the initial, more rapid degradation. Comparing to H_2+H_2O + D4 experiment which contains water with the fuel, the H_2+D4 and H_2+D4+CO experiment have dry fuel and the only source of water is the electrochemical reaction of hydrogen and oxygen in the SOFC.

Besides investigating the degradation in each individual experiment,

degradation comparison among different experiments is also significant in this study. The voltage degradation rate and the ASR increasing rate from Tables 3 and 4 were used as the standard for comparisons. Combined results from polarization and EIS tests indicate the extent of degradation follows the sequence below:

As expected, the H_2+H_2O experiment which was selected as a baseline without D4 had the smallest degradation. However, the dry CO and H_2 fuels with D4 had higher degradation rates than wet H_2 with D4. According to the previous siloxane deposition mechanism, equation (1), this result is unexpected. More details will be discussed in morphology analysis section.

3.2. Morphology analysis

Fig. 4 shows silicon element distribution over the entire anode cross section in which left side is electrolyte and right side is the bottom of anode (fuel inlet). Due to relative weak signal of silicon, the contrast and the brightness of Fig. 4 has been increased to present results clearly. The brightness of the pixels can only be used for silicon distribution analysis and qualitative comparison. The SOFC tested by H_2+H_2O fuel without D4 can be used as a reference sample shown in Fig. 4a. From the figure, there are some silicon spots randomly distributing over the anode's cross section. Those silicon spots are likely due to contamination during fuel cell fabrication instead of D4 deposition. A similar pattern of silicon spots was detected in all of the cross sections. From all the WDS mapping of samples involving D4 in the fuel (Fig. 4b,c,4d), silicon deposition can be detected. The silicon distribution patterns are similar with the bottom of the anode having higher concentration of silicon which gradually decreases in the middle of the anode. From Fig. 4d, some silicon was observed at the electrolyte/anode interface. Higher concentration of silicon around the bottom of the anode, which is near the fuel inlet, indicates that the majority of the silicon is directly deposited after entering fuel cell, far from the active region near the electrolyte. This phenomenon can be explained by higher siloxane concentration around anode bottom, but may also give a hint that the silicon deposition is influenced by the anode materials.

Fig. 5 shows WDS maps of the silicon distribution at small sections of the anode from each experiment. FESEM conditions were kept consistence for all samples to obtain consistent signals. As a result, the silicon deposition around triple boundary areas (Fig. 5a, c, 5e) are similar across all experiments. However, the anode bottom areas (Fig. 5b, d, 5f) have stronger signal. This result coincided with Fig. 4 that silicon was mainly deposited on the bottom of anode. Comparing silicon signals between Fig. 5b, d, f, the fuel cell sample after H_2+ D4 experiment has the strongest silicon signal. The silicon signal in the H_2+H_2O+D4 experiment is weaker and H_2+CO+D4 has the weakest signal for silicon deposition. Part of that trend is consistent with polarization and EIS tests results which showed H_2+D4 experiment degradation rate is higher comparing with H_2+H_2O+D4 experiment.

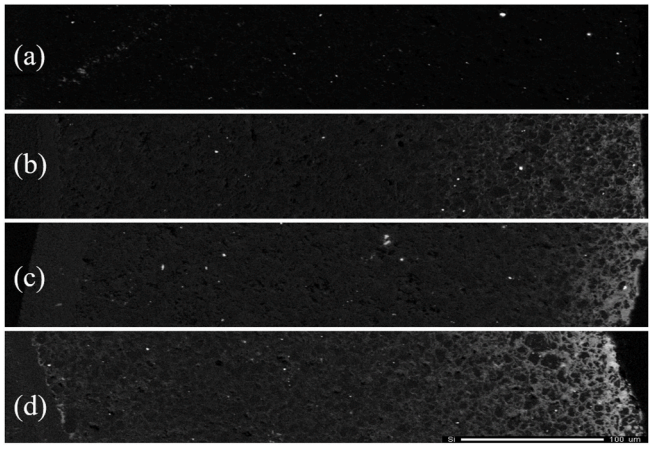

Fig. 4. SEM-WDS mapping of silicon element distribution cross the entire anode after: (a) H_2+H_2O experiment; (b) H_2+D4 experiment; (c) H_2+CO + D4 experiment; (d) H_2+H_2O + D4 experiment. The left sides are YSZ electrolytes and right sides are bottom of anode (fuel inlet).

These results contradict the previous siloxane deposition mechanisms in equation (1), which demonstrate that siloxane reacts with water forming othosilicic acid, and then othosilicic acid dissociates to the silicon dioxide. In this case, the silicon deposition in H_2+H_2O+D4 experiment was expected to be most significant. However, the polarization curves, EIS and SEM-WDS analysis all indicate that the anode will have more degradation due to silicon deposition in H_2+D4 experiment in which the only water source is the product of hydrogen and oxygen reaction. To investigate this phenomenon, 6 μm level SEM-EDS/WDS elemental mapping for anode bottom after H_2+D4 experiment is shown in Fig. 6. It has to be mentioned that when using EDS for the anode, there is signal overlapping between the Y and Si which could cause an overestimate of the Si amount. Supplemental Fig. 3 shows the WDS profile comparison of the anode in a region of low silicon concentration and in high concentration area of silicon to ensure proper silicon detection and separation from Y. For this reason, WDS was used as critical technique to map the location and quantity of the Si in the anode.

From Fig. 6, most carbon and silicon elements are deposited in the pores of the anode. The carbon element is deposited around nickel element significantly. This is verified by examining region 1 labeled in Fig. 6. Compared with the carbon, the silicon element is more associated with yttrium, zirconium and oxygen, which are linked to YSZ. From Fig. 6, the carbon and silicon deposition are noted both coincidentally and separately. Region 2 in Fig. 6 has a large silicon and carbon signal, which may provide a hint that the existence of *Si*–C bond or compounds containing carbon and silicon elements. There is also a large oxygen signal in region 2. To demonstrate the association of silicon, carbon and oxygen and to expose more details, Fig. 7 is presented. In this figure, due to relatively strong signal of oxygen compared with the other two elements, the signal of carbon and silicon were enhanced. As a result, the brightness of each element in this figure can be used for concentration comparison to the relative elements themselves in the same experiment, but not across experiments.

From Fig. 7, the silicon and carbon distributions follow a similar pattern even under three different experiments. Similarly to Figs. 6 and 7 shows that silicon and carbon may deposit individually and coincidentally. Region 1, 2, and 3 in Fig. 7 refer to the bottom of the anode corresponding to H_2+D4, H_2+CO+D4 and H_2+H_2O+D4 experiments, respectively. The overlap of silicon, carbon and oxygen elements can be detected. This result indicates compounds with silicon, carbon and oxygen may still exist in anode. One possibility is that siloxane, which contains C–Si–O bonds, remains intact and directly deposits on the anode. There are also regions that contain only silicon and regions that contain only carbon. Comparing the region near the anode triple boundary layer and anode bottom, the extent of carbon deposition is similar. By contrast, the silicon was mainly deposited on the bottom of anode. This can also be approved by Fig. 4.

3.3. Degradation mechanisms discussions

The results of this study including characterization tests and morphology analysis provide some evidence that contradicts the previously reported mechanism for anode poisoning from siloxane which was mainly attributed to silicon dioxide deposition on the triple phase boundary areas [13,20]. In previous studies it has been shown that as a main product of the thermal degradation of polydimethylsiloxane (PDMS), D4 can exist at high temperature with steam because of its thermodynamic stability [28–30]. According to chemical reaction equation (1), a higher concentration of water should accelerate the siloxane deposition and SOFCs' degradation process. However,

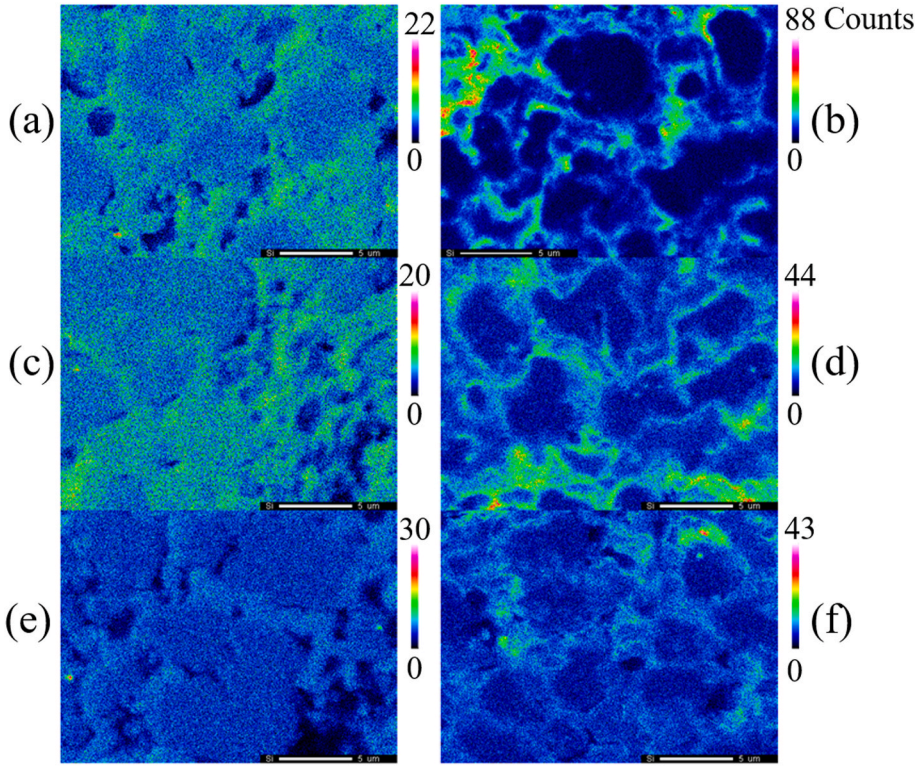

Fig. 5. SEM-WDS mapping of the silicon deposition after experiment on anode: (a) near the triple phase boundary exposed to H_2+D4; (b) near the bottom of anode exposed to H_2+ D4; (c) near the triple phase boundary exposed to H_2+H_2O + D4; (d) near the bottom of anode exposed to H_2+H_2O + D4; (e) near the triple phase boundary exposed to H_2+CO + D4; (f) near the bottom of anode exposed to H_2+CO + D4. (For interpretation of the references to color in this figure legend, the reader is referred to the Web version of this article.)

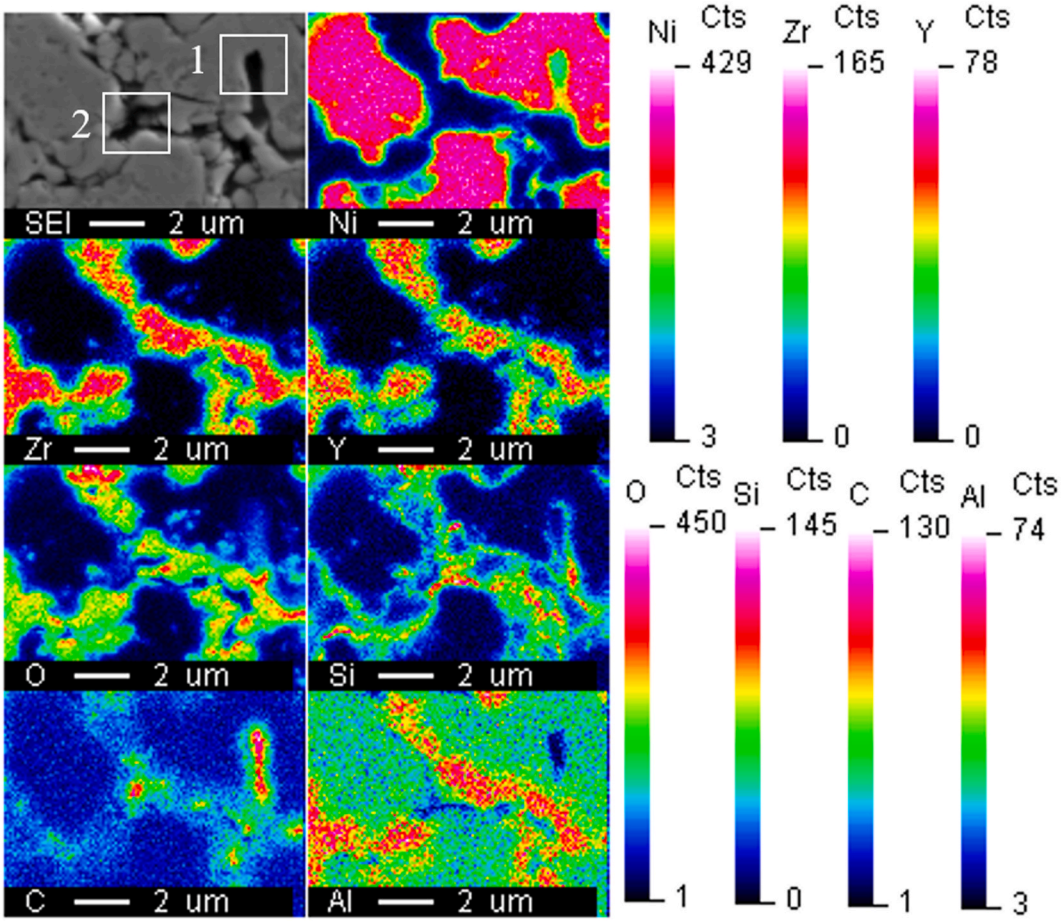

Fig. 6. SEM-EDS/WDS elemental mapping of anode bottom after H_2+ D4 experiment.

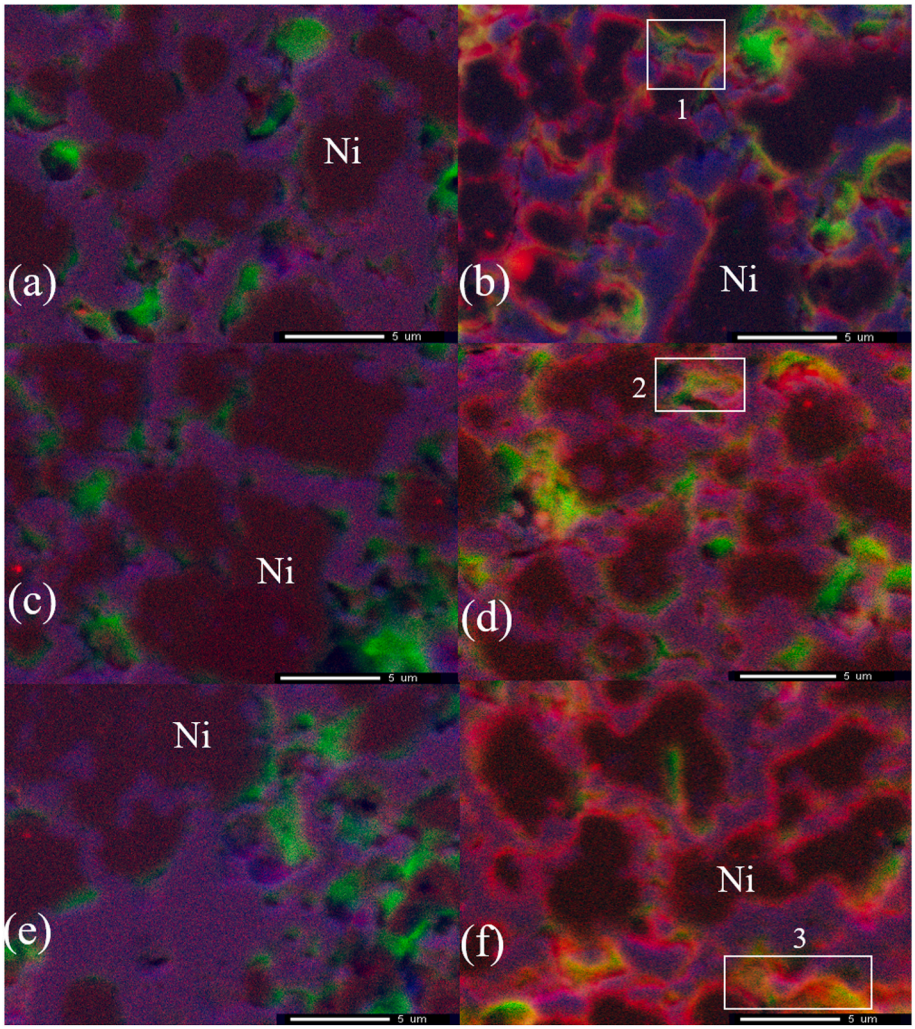

Fig. 7. SEM-EDS/WDS elemental combination mapping after experiment on anode: (a) near the triple phase boundary exposed to H_2+D4; (b) near the bottom of anode exposed to H_2+ D4; (c) near the triple phase boundary exposed to H_2+CO + D4; (d) near the bottom of anode exposed to H_2+CO + D4; (e) near the triple phase boundary exposed to H_2+H_2O + D4; (f) near the bottom of anode exposed to H_2+H_2O + D4. The area of this EDS/WDS map is marked to red color for silicon, blue for oxygen and green for carbon. Dark regions are nickel. (For interpretation of the references to color in this figure legend, the reader is referred to the Web version of this article.)

comparing H_2+H_2O+D4 and H_2+D4 experimental results, feeding with dry fuels with D4 led to more serious degradation and silicon deposition. The H_2+CO+D4 experiment had less silicon deposition with the most severe degradation among all four experiments. From these results, the siloxane poisoning mechanism in SOFCs' anode needs to be discussed again. As valuable references, the mechanism of siloxane deposition on certain metal oxides, like γ-alumina, was investigated previously for biogas cleaning [31]. It is well known that alumina is a good adsorbent of siloxane and has been utilized in industry for siloxane removal. Experimental results indicate that siloxane is first adsorbed to the surface of the metal oxide and the methyl radical in siloxane forms methane according to equation (4) [31].

$$Siloxane\ (g) + bAl_2O_3(s)_{active} \rightarrow silicated\ Al_2O_3(s)_{inert} + xCH_4 \quad (4)$$

Then the other methyl groups in siloxane are converted to methane and replaced by hydroxyl groups. Eventually the siloxane converts to amorphous crystal silicon dioxide [32]. Finocchio and Vaiss et al. [28,33] reported that in the siloxane chemical adsorption process, the surface hydroxyl groups of metal oxide play an important role as shown in equation (5).

$$\gamma - Al_2O_3 - 8OH + [SiO(CH_3)_2]_4 \rightarrow \gamma - Al_2O_3 - 4OH\ Si_4O_8H(CH_3)_5 + 3CH_4 \quad (5)$$

These studies provide evidence for a possible anode degradation mechanism under siloxane contamination. As was shown in Fig. 6, the silicon deposition is mostly associated with the YSZ with little or no silicon in the Ni particles. According to studies from Kogler et al. [34], Y_2O_3 which accounts for 8 mol% in the YSZ used in this study, has a strong initial hydroxylation degree on the surface in a hydrogen atmosphere. In this situation, it shares similar surface hydroxylation properties with Al_2O_3. After dihydroxylation of the Y_2O_3 surface, there are also some mechanisms to recover the hydroxyl groups by hydrogen electro-oxidation reaction on Ni-YSZ anode. The hydrogen spillover mechanism [35] may provide a source of hydroxyl groups shown in equations (6)–(8) [36]. In this circumstance, a new assumed Ni-YSZ SOFC anode degradation mechanism under siloxane contamination is proposed. The first step of the new mechanism is the chemisorption of siloxane on the YSZ surface. The process is shown in Fig. 8 and its chemical reaction equation is given in equation (9).

$$H_2(g) + 2(Ni) \rightleftharpoons 2H(Ni) \quad (6)$$

$$H_2(g) + 2O^{2-}(YSZ) \rightleftharpoons OH^-(YSZ) \quad (7)$$

$$H(Ni) + O^{2-}(YSZ) \rightleftharpoons (Ni) + OH^-(YSZ) + e^-(Ni) \quad (8)$$

$$[(CH_3)_2SiO]_4(g) + 4OH^-(YSZ) \rightleftharpoons Si_4O_8H(CH_3)_5(YSZ) + 3CH_4(g) \quad (9)$$

In the second step, the siloxane adsorbed on the surface of YSZ keeps reacting with hydroxyl groups and releasing methane. Eventually it converts to bulk SiO_2 with surface species SiOH, $Si(OH)_2$, $\equiv SiCH_3$, $=SiOHCH_3$, $=Si(CH_3)_2$, $Si(OX)_4$, $Si(OSi)_3(OX)$ and $Si(OSi)_2(OX)_2$ in which X could be H, Si, Y or Zr. The surface hydroxyl groups provide sites for more siloxane adsorption which eventually lead to SiO_2 as the

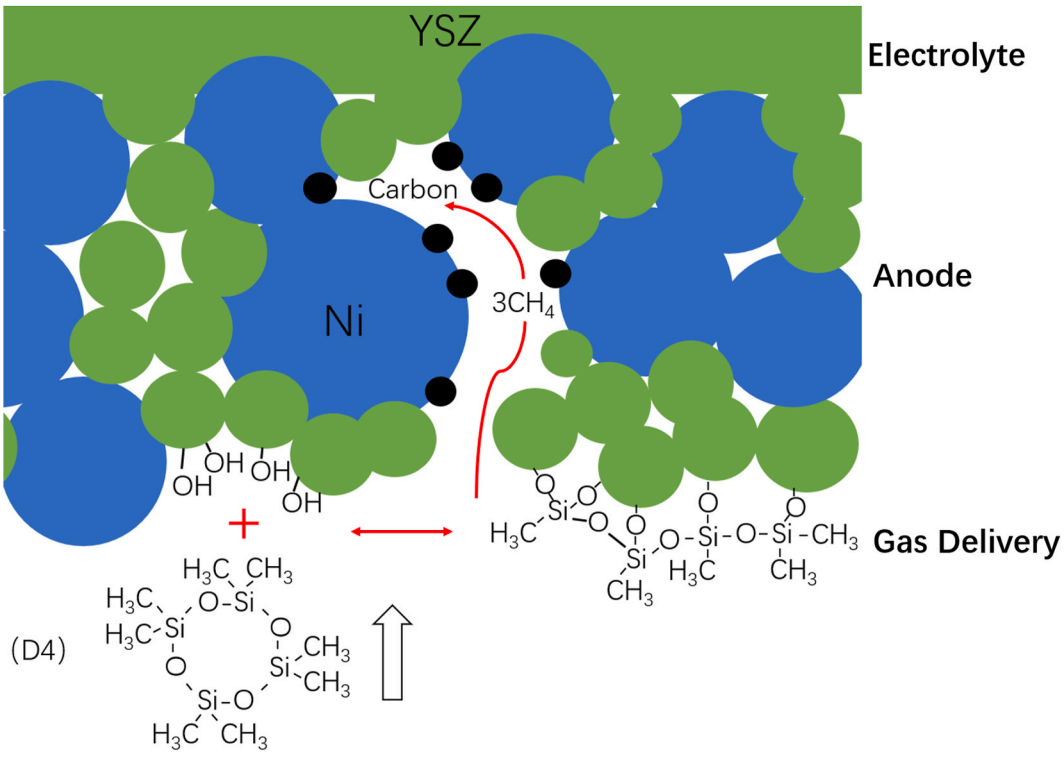

Fig. 8. The early step of assumed Ni-YSZ SOFC anode degradation mechanism under siloxane contamination.

methyl groups are removed. Similar process has been reported by Kellberg and Pérez-Romo et al. for siloxane deposition on alumina [37,38]. This mechanism is supported by the regions of silicon, carbon and oxygen shown in Figs. 6 and 7. These regions represent siloxane that is partially intact. Eventually all of the methyl groups are removed leading to silicon rich (no carbon) regions in Fig. 7. Finocchio et al. [33] reported that existing of water can strongly reduce metal oxide adsorption capacity of siloxane even though it may provide more hydroxyl groups. One reason is that water has a higher tendency to adsorb compared to siloxane [13,33]. A higher concentration of water may also block hydroxyl group recovery path shown in equations (6)–(8). More detailed mechanisms have not been revealed and still require further investigations. This phenomenon can explain the morphology analysis results in Fig. 5 which illustrates that dry H_2+D4 experiment has more silicon deposition at the bottom of the anode than H_2+H_2O+D4 experiment. According to oxygen spillover mechanism [35], the CO electro-oxidation path is show in equations (10)–(12) [39,40]. In this case, a higher concentration of CO can occupy sites on the Ni surface and block hydroxyl group recovery path in H_2 adsorption shown in equation (6). Less hydroxyl groups on the YSZ surface would reduce the siloxane adsorption and finally reduce the deposition. This also explains why less silicon deposition was observed in the H_2+CO+D4 experiment as shown in Fig. 5.

$$CO(g) + (Ni) \rightleftharpoons CO(Ni) \tag{10}$$

$$O_O^x(YSZ) + (YSZ) \rightleftharpoons O^-(YSZ) + V_O^{\cdot\cdot}(YSZ) + e^-(Ni) \tag{11}$$

$$CO(Ni) + O^-(YSZ) \rightleftharpoons CO_2 + (Ni) + (YSZ) + e^-(Ni) \tag{12}$$

Based on the siloxane adsorption mechanism for alumina and the electrochemical reactions in a Ni + YSZ anode, the proceeding discussion and experimental results provide evidence for reaction equation (9). This mechanism can also explain the regions with only carbon deposition (no silicon deposition) observed in the experiments. Carbon deposition from direct use of methane with a Ni based anode is widely reported. Methane released from siloxane can result in carbon deposition on Ni. The possible deposition equation is shown in equation (13) [41,42]. It also can be supported by the carbon deposition region near the nickel particles in Fig. 6 region 1. Different from the previous studies, the siloxane contamination mechanism in this study proposes that the anode degradation occurs by deposition of silicon and carbon. This new mechanism can explain the morphology analysis results in Fig. 6 which shows that silicon deposition is overlapped to the YSZ and carbon associating to nickel particles. Methane, as the products of siloxane chemical adsorption and demethylation in equation (9), has an ability to penetrate through the anode and deposit on nickel even in the vicinity of YSZ electrolyte where there is more active electrochemical reactions. This possibility is supported by the existence of carbon deposition near the electrolyte in Fig. 7. The carbon deposition can also provide an explanation for the large degradation in the H_2+D4 experiment which suffered more degradation compared with H_2+H_2O+D4 experiment. According to research by Koh et al. [43], supplying dry methane to Ni-YSZ anode would cause irreversible carbon deposition. In contrast, wet methane results in reversible deposition. Ni is also considered as an excellent catalyst for methane reforming reaction shown in equation (14), in which carbon in methane is converted to CO, thus avoiding deposit directly [44]. In this regard, H_2+H_2O+D4 experiment involving water in the fuel would have less carbon deposition and less anode degradation. All EIS results with dry fuel including H_2+D4 and H_2+CO+D4 experiment show that the rate of increase of ohmic resistance is proportional to the D4 concentrations. This can be explained by the proposed mechanism as carbon deposits on Ni which acts as the conductor in anode. Carbon deposition between the grain boundaries of Ni can lead to this increase in ohmic resistance.

$$CH_4 \rightarrow 2H_2 + C \tag{13}$$

$$CH_4 + H_2O \rightarrow 3H_2 + CO \tag{14}$$

The siloxane deposition mechanism in this study suggests multi-step silicon deposition and also highlights the importance of carbon deposition. As shown, the complexity of the entire degradation process is enhanced dramatically. The degradation results should be analyzed

comprehensively, not with silicon or carbon deposition individually. Under this premise, some inexplicable results presented before can be assessed. According to Figs. 4 and 7, the silicon is mainly deposited near the bottom of the anode near the fuel inlet. However, significant carbon deposition is observed inside the anode due to methane transportation. The chemical adsorption of siloxane on the YSZ surface is the first step which should be responsible for initial anode degradation. Following the adsorption process, the siloxane is gradually converted to SiO_2. From the second step, the pores around the bottom of the anode shrink, which hinders gas delivery. Although these two steps cause anode degradation, compared with carbon deposition their position is far from the electrolyte where the main electrochemical active region is located. This may explain why the experiment with dry fuel had relative low degradation rate initially and higher degradation rate later due to carbon deposition. Water inhibits the carbon deposition which reduces the degradation rate of experiments with wet fuel. The H_2+CO+D4 experiment has less silicon deposition, but the most performance degradation. This phenomenon may also result from carbon deposition originating from CO. Carbon deposition from CO can result from two different pathways shown in equations (15) and (16) [45].

$$2CO \rightarrow CO_2 + C \quad (15)$$

$$CO + H_2 \rightarrow H_2O + C \quad (16)$$

4. Conclusions

In order to reveal the Ni-YSZ anode degradation mechanism exposed to siloxane (D4), which is one of main impurities in biogas, long term experiments with H_2+H_2O, H_2+H_2O+D4, H_2+D4 and H_2+CO+D4 as fuels are reported. The electrochemical characterization and morphology results of different experiments were analyzed and compared to investigate the degradation phenomenon.

Based on electrochemical characterization results, the degradation rates of different experiments were following the sequence with: H_2+D4+CO experiment > H_2+D4 experiment > H_2+H_2O+D4 experiment > H_2+H_2O experiment. The results also show that the initial degradation rates were more likely time dependent rather than D4 concentration dependent.

According to morphology analysis the silicon deposition, which mainly occurred around bottom (fuel inlet) side of anode can be detected when the fuels were mixed with D4. The H_2+D4 experiment with dry fuel has more serious silicon deposition comparing with H_2+H_2O+D4 experiment. And the H_2+CO+D4 experiment has the lowest silicon deposition extent besides the H_2+H_2O experiment. Similar amounts of carbon deposition was also detected both at the bottom (fuel inlet) side and in vicinity of YSZ electrolyte. Except silicon and carbon depositing individually, the overlap of silicon, carbon and oxygen was also noticed, which indicated the combination of these elements possibly as intact siloxane.

The results presented contradict the previous Ni-YSZ SOFC anode degradation mechanism by siloxane, in which siloxane reacts with water and then deposits in the anode. The SOFC in the H_2+H_2O+D4 experiment of this study has less performance degradation and less silicon deposition than H_2+D4 experiment. In this situation, a new multi-step degradation mechanism has been proposed that the siloxane adsorbs and deposits on the YSZ surface. The methane releasing from previous two steps would cause carbon deposition on the Ni surface. In this mechanism, the silicon and carbon deposition are both essential factors resulting in anode degradation.

CRediT authorship contribution statement

Jiashen Tian: Conceptualization, Methodology, Validation, Investigation, Writing - original draft, Writing - review & editing. **Ryan J. Milcarek:** Conceptualization, Methodology, Validation, Investigation, Writing - original draft, Writing - review & editing, Supervision, Funding acquisition.

Declaration of competing interest

The authors declare that they have no known competing financial interests or personal relationships that could have appeared to influence the work reported in this paper.

Acknowledgement

This material is based upon work supported by the U.S. Department of Energy under award number DE-EE0007721. We acknowledge the use of facilities within the Eyring Materials Center at Arizona State University supported in part by NNCI-ECCS-1542160.

Appendix A. Supplementary data

Supplementary data to this article can be found online at https://doi.org/10.1016/j.jpowsour.2020.229122.

References

[1] Y. Shen, J.L. Linville, M. Urgun-Demirtas, R.P. Schoene, S.W. Snyder, Producing pipeline-quality biomethane via anaerobic digestion of sludge amended with corn stover biochar with in-situ CO_2 removal, Appl. Energy 158 (2015) 300–309, https://doi.org/10.1016/j.apenergy.2015.08.016.
[2] C. Goff, Combined Heat and Power at Wastewater Treatment Facilities : Market Analysis and Lessons from the EPA & Combined Heat and Power, 2011.
[3] M. Gandiglio, A. Lanzini, M. Santarelli, M. Acri, T. Hakala, M. Rautanen, Results from an industrial size biogas-fed SOFC plant (the DEMOSOFC project), Int. J. Hydrogen Energy 45 (2020) 5449–5464, https://doi.org/10.1016/j.ijhydene.2019.08.022.
[4] E. Rillo, M. Gandiglio, A. Lanzini, S. Bobba, M. Santarelli, G. Blengini, Life cycle assessment (LCA) of biogas-fed solid oxide fuel cell (SOFC) plant, Energy 126 (2017) 585–602, https://doi.org/10.1016/j.energy.2017.03.041.
[5] D. Papurello, A. Lanzini, SOFC single cells fed by biogas: experimental tests with trace contaminants, Waste Manag. 72 (2018) 306–312, https://doi.org/10.1016/j.wasman.2017.11.030.
[6] E. Ryckebosch, M. Drouillon, H. Vervaeren, Techniques for transformation of biogas to biomethane, Biomass Bioenergy 35 (2011) 1633–1645, https://doi.org/10.1016/j.biombioe.2011.02.033.
[7] D. Papurello, A. Lanzini, D. Drago, P. Leone, M. Santarelli, Limiting factors for planar solid oxide fuel cells under different trace compound concentrations, Energy 95 (2016) 67–78, https://doi.org/10.1016/j.energy.2015.11.070.
[8] D. Papurello, R. Borchiellini, P. Bareschino, V. Chiodo, S. Freni, A. Lanzini, F. Pepe, G.A. Ortigoza, M. Santarelli, Performance of a solid oxide fuel cell short-stack with biogas feeding, Appl. Energy 125 (2014) 254–263, https://doi.org/10.1016/j.apenergy.2014.03.040.
[9] D.D. Papadias, S. Ahmed, R. Kumar, Fuel quality issues with biogas energy – an economic analysis for a stationary fuel cell system, Energy 44 (2012) 257–277, https://doi.org/10.1016/j.energy.2012.06.031.
[10] J. Álvarez-Flórez, E. Egusquiza, Analysis of damage caused by siloxanes in stationary reciprocating internal combustion engines operating with landfill gas, Eng. Fail. Anal. 50 (2015) 29–38, https://doi.org/10.1016/j.engfailanal.2015.01.010.
[11] E. Wheless, J. Pierce, Siloxanes in landfill and digester gas update, SCS Eng. Environ. Consult. Contract (2004) 1–10. http://mercmail.scsengineers.com/Papers/Pierce_2004Siloxanes_Update_Paper.pdf.
[12] M. Arnold, VTT RESEARCH NOTES 2496 Reduction and Monitoring of Biogas Trace Compounds, 2006. http://www.vtt.fi/publications/index.jsp.
[13] A. Lanzini, J. Van herle, J. Gutzon Larsen, M. Lualdi, M. Santarelli, D. Papurello, H. Madi, S. Diethelm, Solid oxide fuel cell anode degradation by the effect of siloxanes, J. Power Sources 279 (2015) 460–471, https://doi.org/10.1016/j.jpowsour.2015.01.053.
[14] A. Lanzini, H. Madi, V. Chiodo, D. Papurello, S. Maisano, M. Santarelli, J. Van herle, Dealing with fuel contaminants in biogas-fed solid oxide fuel cell (SOFC) and molten carbonate fuel cell (MCFC) plants: degradation of catalytic and electrocatalytic active surfaces and related gas purification methods, Prog. Energy Combust. Sci. 61 (2017) 150–188, https://doi.org/10.1016/j.pecs.2017.04.002.
[15] H. Wasajja, R.E.F. Lindeboom, J.B. van Lier, P.V. Aravind, Techno-economic review of biogas cleaning technologies for small scale off-grid solid oxide fuel cell applications, Fuel Process, Technol. 197 (2020) 106215, https://doi.org/10.1016/j.fuproc.2019.106215.
[16] C. Rücker, K. Kümmerer, Environmental chemistry of organosiloxanes, Chem. Rev. 115 (2015) 466–524, https://doi.org/10.1021/cr500319v.
[17] H. Madi, S. Diethelm, S. Poitel, C. Ludwig, J. Van herle, Damage of siloxanes on Ni-YSZ anode supported SOFC operated on hydrogen and bio-syngas, Fuel Cell. 15 (2015) 718–727, https://doi.org/10.1002/fuce.201400185.

[18] R. Dewil, L. Appels, J. Baeyens, Energy use of biogas hampered by the presence of siloxanes, Energy Convers. Manag. 47 (2006) 1711–1722, https://doi.org/10.1016/j.enconman.2005.10.016.
[19] J. Rossmeisl, W.G. Bessler, Trends in catalytic activity for SOFC anode materials, Solid State Ionics 178 (2008) 1694–1700, https://doi.org/10.1016/j.ssi.2007.10.016.
[20] K. Haga, S. Adachi, Y. Shiratori, K. Itoh, K. Sasaki, Poisoning of SOFC anodes by various fuel impurities, Solid State Ionics 179 (2008) 1427–1431, https://doi.org/10.1016/j.ssi.2008.02.062.
[21] K. Sasaki, K. Haga, T. Yoshizumi, D. Minematsu, E. Yuki, R.-R. Liu, C. Uryu, T. Oshima, S. Taniguchi, Y. Shiratori, K. Ito, Impurity poisoning of SOFCs, ECS Trans 35 (2019) 2805–2814, https://doi.org/10.1149/1.3570280.
[22] K. Haga, Y. Shiratori, K. Ito, K. Sasaki, Chemical degradation and poisoning mechanism of cermet anodes in solid oxide fuel cells, ECS Trans 25 (2019) 2031–2038, https://doi.org/10.1149/1.3205748.
[23] Y. Kikuchi, J. Matsuda, Y. Tachikawa, Y. Shiratori, S. Taniguchi, K. Sasaki, Degradation of SOFCs by various impurities: impedance spectroscopy and microstructural analysis, ECS Trans 78 (2017) 1253–1260, https://doi.org/10.1149/07801.1253ecst.
[24] R.J. Milcarek, K. Wang, M.J. Garrett, J. Ahn, Performance investigation of dual layer yttria-stabilized zirconia-samaria-doped ceria electrolyte for intermediate temperature solid oxide fuel cells, J. Electrochem. Energy Convers. Storage. 13 (2016) 31–32, https://doi.org/10.1115/1.4032708.
[25] R.J. Milcarek, K. Wang, R.L. Falkenstein-Smith, J. Ahn, Performance variation with SDC buffer layer thickness, Int. J. Hydrogen Energy 41 (2016) 9500–9506, https://doi.org/10.1016/j.ijhydene.2016.04.113.
[26] C. Comminges, Q.X. Fu, M. Zahid, N.Y. Steiner, O. Bucheli, Monitoring the degradation of a solid oxide fuel cell stack during 10,000 h via electrochemical impedance spectroscopy, Electrochim. Acta 59 (2012) 367–375, https://doi.org/10.1016/j.electacta.2011.10.080.
[27] C. Sun, R. Hui, J. Roller, Cathode materials for solid oxide fuel cells: a review, J. Solid State Electrochem. 14 (2010) 1125–1144, https://doi.org/10.1007/s10008-009-0932-0.
[28] V.S. Vaiss, C.G. Fonseca, F.P.N. Antunes, L.S. Chinelatto Jr., S.S.X. Chiaro, W. F. Souza, A.A. Leitão, Experimental and theoretical study of deactivated HDT catalysts by Si species deposited on their surfaces: models proposition, structural and thermodynamic analysis, J. Catal. 389 (2020) 578–591, https://doi.org/10.1016/j.jcat.2020.06.007.
[29] F. Chainet, M. Courtiade, C.P. Lienemann, J. Ponthus, O.F.X. Donard, Silicon speciation by gas chromatography coupled to mass spectrometry in gasolines, J. Chromatogr., A 1218 (2011) 9269–9278, https://doi.org/10.1016/j.chroma.2011.10.047.
[30] F. Chainet, C.P. Lienemann, J. Ponthus, M. Courtiade, O.F.X. Donard, Development of heart-cutting multidimensional gas chromatography coupled to time of flight mass spectrometry for silicon speciation at trace levels in gasoline samples, J. Chromatogr., A 1264 (2012) 80–86, https://doi.org/10.1016/j.chroma.2012.09.020.
[31] A.C. Sonoc, C. Thurgood, B. Peppley, D.G. Kelly, Kinetic study of the thermal decomposition of octamethylcyclotetrasiloxane on activated gamma alumina, J. Environ. Chem. Eng. 5 (2017) 4858–4865, https://doi.org/10.1016/j.jece.2017.07.057.
[32] N.H. Elsayed, A. Elwell, B. Joseph, J.N. Kuhn, Effect of silicon poisoning on catalytic dry reforming of simulated biogas, Appl. Catal. Gen. 538 (2017) 157–164, https://doi.org/10.1016/j.apcata.2017.03.024.
[33] E. Finocchio, G. Garuti, M. Baldi, G. Busca, Decomposition of hexamethylcyclotrisiloxane over solid oxides, Chemosphere 72 (2008) 1659–1663, https://doi.org/10.1016/j.chemosphere.2008.05.032.
[34] M. Kogler, E.M. Köck, T. Bielz, K. Pfaller, B. Klötzer, D. Schmidmair, L. Perfler, S. Penner, Hydrogen surface reactions and adsorption studied on Y_2O_3, YSZ, and ZrO_2, J. Phys. Chem. C 118 (2014) 8435–8444, https://doi.org/10.1021/jp5008472.
[35] K. Ong, J. Hanna, A.F. Ghoniem, Investigation of a combined hydrogen and oxygen spillover mechanism for syngas electro-oxidation on Ni/YSZ, J. Electrochem. Soc. 164 (2016) F32, https://doi.org/10.1149/2.0161702jes. F45.
[36] H. Zhu, R.J. Kee, V.M. Janardhanan, O. Deutschmann, D.G. Goodwin, Modeling elementary heterogeneous chemistry and electrochemistry in solid-oxide fuel cells, J. Electrochem. Soc. 152 (2005) A2427, https://doi.org/10.1149/1.2116607.
[37] L. Kellberg, P. Zeuthen, H.J. Jakobsen, Deactivation of HDT catalysts by formation of silica gels from silicone oil. Characterization of spent catalysts from HDT of coker naphtha using ^{29}Si and ^{13}C CP/MAS NMR, J. Catal. 143 (1993) 45–51, https://doi.org/10.1006/jcat.1993.1252.
[38] P. Pérez-Romo, J. Navarrete-Bolaños, C. Aguilar-Barrera, C. Angeles-Chavez, G. C. Laredo, Morphological and structural study of the Si deposition on the sulfided NiMo/γ-Al_2O_3 catalyst: effect on the support, Appl. Catal. Gen. 485 (2014) 84–90, https://doi.org/10.1016/j.apcata.2014.07.038.
[39] J. Hanna, W.Y. Lee, A.F. Ghoniem, Kinetics of carbon monoxide electro-oxidation in solid-oxide fuel cells from Ni-YSZ patterned-anode measurements, J. Electrochem. Soc. 160 (2013) F698–F708, https://doi.org/10.1149/2.136606jes.
[40] V. Yurkiv, D. Starukhin, H.-R. Volpp, W.G. Bessler, Elementary reaction kinetics of the $CO/CO_2/Ni/YSZ$ electrode, J. Electrochem. Soc. 158 (2011), https://doi.org/10.1149/1.3505296. B5.
[41] R.J. Milcarek, J. Ahn, Micro-tubular flame-assisted fuel cells running methane, propane and butane: on soot, efficiency and power density, Energy 169 (2019) 776–782, https://doi.org/10.1016/j.energy.2018.12.098.
[42] E. Achenbach, Three-dimensional and time-dependent simulation of a planar solid oxide fuel cell stack, J. Power Sources 49 (1994) 333–348, https://doi.org/10.1016/0378-7753(93)01833-4.
[43] J.H. Koh, Y.S. Yoo, J.W. Park, H.C. Lim, Carbon deposition and cell performance of Ni-YSZ anode support SOFC with methane fuel, Solid State Ionics 149 (2002) 157–166, https://doi.org/10.1016/S0167-2738(02)00243-6.
[44] E.S. Hecht, G.K. Gupta, H. Zhu, A.M. Dean, R.J. Kee, L. Maier, O. Deutschmann, Methane reforming kinetics within a Ni-YSZ SOFC anode support, Appl. Catal. Gen. 295 (2005) 40–51, https://doi.org/10.1016/j.apcata.2005.08.003.
[45] S. Farhad, F. Hamdullahpur, Y. Yoo, Performance evaluation of different configurations of biogas-fuelled SOFC micro-CHP systems for residential applications, Int. J. Hydrogen Energy 35 (2010) 3758–3768, https://doi.org/10.1016/j.ijhydene.2010.01.052.

Glossary

ASR: Area specific resistance
AS-SOFCs: Anode supported solid oxide fuel cells
CHP: Combined heat and power
D4: Octamethylcyclotetrasiloxane
D5: Decamethylcyclopentasiloxane
EDS: Energy-dispersive spectrometer
EIS: Electrochemical impedance spectroscopy
FESEM: Field emission scanning electron microscope
I–V: Current-voltage
L3: Octamethyltrisiloxane
L4: Decamethyltetrasiloxane
LSCF: lanthanum strontium cobalt ferrite, $(La_{0.60}Sr_{0.40})_{0.95}Co_{0.20}Fe_{0.80}O_{3-x}$
MFCs: Mass flow controllers
OCV: Open circuit voltage
PDMS: Polydimethylsiloxane
ppm: Parts per million
sccm: Standard cubic centimeters per minute
SDC: Samarium doped ceria, $Sm_{0.20}Ce_{0.80}O_{2-X}$
SOFC: Solid oxide fuel cell
TMS: Trimethylsilanol
TPB: Triple phase boundary
vol%: Volume percent
V-t curve: Voltage versus time curve
WDS: Wavelength-dispersive spectrometers
WWTPs: Water and wastewater treatment plants
YSZ: Yttria-stabilized zirconia, $(ZrO_2)_{0.92}(Y_2O_3)_{0.08}$